

Parsec-scale jet precession in BL Lacertae (2200+420)

A. Caproni^{1*}, Z. Abraham² and H. Monteiro³

¹*Núcleo de Astrofísica Teórica, Universidade Cruzeiro do Sul, R. Galvão Bueno 868, Liberdade, 01506-000, São Paulo, SP, Brazil*

²*Instituto de Astronomia, Geofísica e Ciências Atmosféricas, Universidade de São Paulo, R. do Matão 1226, Cidade Universitária, 05508-900, São Paulo, SP, Brazil*

³*UNIFEI, Instituto de Ciências Exatas, Universidade Federal de Itajubá, Av. BPS 1303, Pinheirinho, 37500-903, Itajubá, MG, Brazil*

Accepted 1988 December 15. Received 1988 December 14; in original form 1988 October 11

ABSTRACT

BL Lacertae is the prototype of the BL Lac class of active galactic nuclei, exhibiting intensive activity on parsec (pc) scales, such as intense core variability and multiple ejections of jet components. In particular, in previous works the existence of precession motions in the pc-scale jet of BL Lacertae has been suggested. In this work we revisit this issue, investigating temporal changes of the observed right ascension and declination offsets of the jet knots in terms of our relativistic jet-precession model. The seven free parameters of our precession model were optimized via a heuristic cross-entropy method, comparing the projected precession helix with the positions of the jet components on the plane of the sky and imposing constraints on their maximum and minimum superluminal velocities. Our optimized best model is compatible with a jet having a bulk velocity of $0.9824c$, which is precessing with a period of about 12.1 yr in the observers reference frame and changing its orientation in relation to the line of sight between 4° and 5° , approximately. Assuming that the jet precession has its origin in a supermassive binary black hole system, we show that the 2.3-yr periodic variation in the structural position angle of the very-long-baseline interferometry (VLBI) core of BL Lacertae reported by Stirling et al. is compatible with a nutation phenomenon if the secondary black hole has a mass higher than about six times that of the primary black hole.

Key words: galaxies: active – BL Lacertae objects: individual: (BL Lacertae) – galaxies: jets – radio continuum: galaxies.

1 INTRODUCTION

BL Lacertae or 2200+420 ($z=0.0686$; Vermeulen et al. 1995), the prototype of the BL Lac class of active galactic nuclei, is hosted by an elliptical galaxy, composed mainly by a stellar population of about 0.7 Gyr (Hyvönen et al. 2007). As usual in BL Lac type objects, its nuclear region exhibits strong continuum variability on different time-scales, from days to years, over the whole electromagnetic spectrum.

High-resolution interferometric images at radio wavelengths show the presence of a compact core and a diffuse halo-like source at arc-second scales (Antonucci 1986). At an intermediate resolution (~ 10 mas), BL Lacertae shows a core-jet structure, with components following different trajectories on the plane of the sky (Polatidis et al. 1995). Similar behavior is seen at mas resolution, which has been attributed to either helical instabilities (e.g., Tateyama et al. 1998; Denn, Mutel & Marscher 2000) or jet inlet precession (Stirling et al. 2003; Tateyama 2009). Concerning jet pre-

cession, Stirling et al. (2003) proposed a period of 2.29 years based on the periodic variations in the polarization position angle at 1 mm, and in the direction of the innermost radio core component at 43 GHz, which has been matter of criticism in some recent works (e.g., Mutel & Denn 2005). Tateyama (2009) proposed an alternative precession model in which the BL Lacertae parsec-scale jet changes its orientation in a period of about 26 yr. Such claim was based on analyses of maps of BL Lacertae at 8 and 15 GHz in a super-resolution mode.

In this work, we reanalyse the jet-precession proposition in terms of our ballistic jet precession model, described in Section 2. In Section 3, we introduce the cross-entropy (CE) global optimization technique in the context of our precession model. In Section 4, we show the general results from the application of our CE jet-precession model to BL Lacertae, as well as the observational constraints used in this work. We explore in Section 5 the possible consequences of the underlying jet intensity on the radio and optical historical light curves. In Section 6 we study the viability of a supermassive binary black hole system in the nuclear region

* E-mail: anderson.caproni@cruzeirodosul.edu.br

of BL Lacertae in producing the inferred jet precession rate, as well as a nutation motion with period of 2.3 yr. Finally, general conclusions are presented in Section 7.

We will assume throughout this work a Λ CDM cosmology with $H_0 = 71 \text{ km s}^{-1} \text{ Mpc}^{-1}$, $\Omega_M = 0.27$, and $\Omega_\Lambda = 0.73$, which implies $1 \text{ mas} = 1.296 \text{ pc}$ and $1 \text{ mas yr}^{-1} = 4.516c$ for BL Lacertae.

2 BALLISTIC JET PRECESSION MODEL

Let us consider a relativistic jet receding from the core with a constant bulk velocity β (in units of the speed of light c) that precesses around a fixed axis (see Fig. 1 in Caproni, Monteiro & Abraham 2009 for a schematic representation of this). Precession makes the jet inlet direction vary with time with a precession period $P_{\text{prec},s}$ measured in the source reference frame, producing a cone with semi-aperture angle φ_0 . The precession phase $\omega_s \Delta t_s = 2\pi(t_s - t_{0,s})/P_{\text{prec},s} = 2\pi(\tau_s - \tau_{0,s})$ is chosen arbitrarily to be zero on the $y_s z_s$ -plane at $\tau_s = \tau_{0,s}$ (Caproni, Monteiro & Abraham 2009). From these definitions, the instantaneous jet inlet direction is given in terms of a unit vector with Cartesian components:

$$e_{x,s}(\tau_s) = \sin \varphi_0 \sin[\iota 2\pi(\tau_s - \tau_{0,s})],$$

$$e_{y,s}(\tau_s) = \sin \varphi_0 \cos[\iota 2\pi(\tau_s - \tau_{0,s})],$$

$$e_{z,s}(\tau_s) = \cos \varphi_0,$$

where ι gives the sense of precession, $\iota = 1$ for clockwise sense and $\iota = -1$ for counterclockwise precession.

Introducing the parameters ϕ_0 , the angle between the precession cone axis and the line of sight, and η_0 , the position angle of the axis on the plane of the sky (positive from north to east), we have (e.g., Caproni & Abraham 2004a,b; Caproni, Monteiro & Abraham 2009):

$$e_{x,\text{obs}}(\tau_s) = A(\tau_s) \cos \eta_0 - e_{y,s}(\tau_s) \sin \eta_0, \quad (1)$$

$$e_{y,\text{obs}}(\tau_s) = A(\tau_s) \sin \eta_0 + e_{y,s}(\tau_s) \cos \eta_0, \quad (2)$$

$$e_{z,\text{obs}}(\tau_s) = -e_{x,s}(\tau_s) \sin \phi_0 + e_{z,s}(\tau_s) \cos \phi_0, \quad (3)$$

where:

$$A(\tau_s) = e_{x,s}(\tau_s) \cos \phi_0 + e_{z,s}(\tau_s) \sin \phi_0. \quad (4)$$

The instantaneous angle between the jet and the line of sight ϕ is calculated from:

$$\phi(\tau_s) = \arccos[e_{z,\text{obs}}(\tau_s)], \quad (5)$$

while the position angle of the jet on the plane of the sky η is obtained from:

$$\eta(\tau_s) = \arctan \left[\frac{e_{y,\text{obs}}(\tau_s)}{e_{x,\text{obs}}(\tau_s)} \right]. \quad (6)$$

The observed jet velocity $\beta_{\text{obs}}(\tau_s)$ is:

$$\beta_{\text{obs}}(\tau_s) = \gamma \beta \delta(\tau_s) \sin \phi(\tau_s), \quad (7)$$

where the jet Lorentz factor γ is

$$\gamma = (1 - \beta^2)^{-1/2}, \quad (8)$$

and the jet Doppler factor δ is:

$$\delta(\tau_s) = \gamma^{-1} [1 - \beta \cos \phi(\tau_s)]^{-1}. \quad (9)$$

In order to compare predictions from the precession model with observational data, it is necessary to transform the elapsed time measured in the source's reference frame dt_s to the time interval in the observer's framework dt_{obs} . Following Gower et al. (1982) and Caproni, Monteiro & Abraham (2009), we can write:

$$\frac{\Delta t_{\text{obs}}}{P_{\text{prec,obs}}} = \frac{\int_0^{\Delta \tau_s} \delta^{-1}(\tau) d\tau}{\int_0^1 \delta^{-1}(\tau) d\tau}, \quad (10)$$

where $\Delta t_{\text{obs}} = (t_{\text{obs}} - t_{0,\text{obs}})$ and $\Delta \tau_s = \tau_s - \tau_{0,s}$.

The relation between the precession period in the source's framework and that measured by the observer $P_{\text{prec,obs}}$ is given as:

$$P_{\text{prec},s} = \frac{\gamma}{(1+z)} \frac{P_{\text{prec,obs}}}{\int_0^1 \delta^{-1}(\tau) d\tau}, \quad (11)$$

where z is the redshift of the source.

A fluid element of the jet, ejected at time $t_{\text{obs,ej}}$ from a jet inlet region that is precessing according to our model, will be observed at time t_{obs} with right ascension and declination offsets from the core $\Delta \alpha_{\text{mod}}$ and $\Delta \delta_{\text{mod}}$ respectively, given by:

$$\Delta \alpha_{\text{mod}}(t_{\text{obs}}) = (t_{\text{obs}} - t_{\text{obs,ej}}) \mu(t_{\text{obs,ej}}) \sin[\eta(t_{\text{obs,ej}})], \quad (12)$$

$$\Delta \delta_{\text{mod}}(t_{\text{obs}}) = (t_{\text{obs}} - t_{\text{obs,ej}}) \mu(t_{\text{obs,ej}}) \cos[\eta(t_{\text{obs,ej}})], \quad (13)$$

where μ is the proper motion of the fluid element predicted by our jet-precession model assuming outward motion at a constant speed.

Considering all the possible values of $t_{\text{obs,ej}} < t_{\text{obs}}$ we obtain a snapshot of the model jet at time t_{obs} , projected on the plane of the sky. The real jet, as observed with VLBI techniques, is not continuous but formed by discrete components, ejected at unknown epochs with unknown velocities. To avoid incorrect identifications of the same component in maps obtained at different epochs (which could lead to incorrect determination of $t_{\text{obs,ej}}$ and $\mu(t_{\text{obs,ej}})$ for this component), we will use only the projected position of the components in the plane of the sky for each epoch in which a map is available, and compare them with the positions predicted by the model.

In summary, our jet precession model has seven free parameters ($P_{\text{prec,obs}}$, ι , γ , η_0 , ϕ_0 , φ_0 and $\tau_{0,s}$), which are determined, via the CE technique as will be discussed in the next Section.

3 THE CROSS-ENTROPY PRECESSION METHOD

3.1 General overview

The CE method was originally employed in the optimization of complex computer simulation models involving rare events simulations (Rubinstein 1997), having been modified by Rubinstein (1999) to deal with continuous multi-extremal and discrete combinatorial optimization problems. Its theoretical asymptotic convergence in such situations has been demonstrated by Margolin (2004), while Kroese, Porotsky & Rubinstein (2006) studied the efficiency of the CE method in solving continuous multi-extremal optimization problems. Some examples of robustness of the

CE method in several situations are listed in de Boer et al (2005).

CE optimization involves basically random generation of the initial parameter sample (obeying some predefined criteria) and selection of the best samples based on some mathematical criterion. Subsequent random generation of updated parameter samples from the previous best candidates are performed iteration by iteration until a pre-specified stopping criterion is fulfilled.

Application of the CE method in astrophysical contexts can be found in Caproni, Monteiro & Abraham (2009), Monteiro et al. (2010), Caproni et al. (2011) and Monteiro & Dias (2011).

3.2 Our CE algorithm for jet precession modelling

Following Caproni, Monteiro & Abraham (2009), let us suppose that we wish to study a set of N_d observational data in terms of an analytical model characterized by N_p parameters p_1, p_2, \dots, p_{N_p} . In the case of jet precession modelling, the observational data correspond to right ascension and declination offsets, $\Delta\alpha$ and $\Delta\delta$ respectively, for the N_d knots. As mentioned before, our precession model is defined by the free parameters β (or γ), η_0 , ϕ_0 , φ_0 , $\tau_{0,s}$, $P_{\text{prec,obs}}$ (or $P_{\text{prec,s}}$) and ι , i.e., $N_p = 7$. In this work, we adopted the same procedure suggested by Caproni, Monteiro & Abraham (2009), in which for a given (fixed) value of $P_{\text{prec,obs}}$ and ι , the remaining five parameters are CE optimized. Therefore, it is necessary to test different values for the precession period, as well as distinct senses of precession in order to obtain the best set of model parameters.

The main goal of the CE continuous multi-extremal optimization method is to find the set of parameters $\mathbf{x}^* = (p_1^*, p_2^*, \dots, p_{N_p}^*)$ for which the model provides the best description of the data (Rubinstein 1999; Kroese, Porotsky & Rubinstein 2006). It is performed generating randomly N independent sets of model parameters $\mathbf{X} = (\mathbf{x}_1, \mathbf{x}_2, \dots, \mathbf{x}_N)$, where $\mathbf{x}_i = (p_{1i}, p_{2i}, \dots, p_{N_{pi}})$, and minimizing a merit function $S(\mathbf{x})$ used to transmit the quality of the fit during the run process. If the convergence to the exact solution is achieved then $S(\mathbf{x}^*) \rightarrow 0$.

In order to find the optimal solution from CE optimization, we start by defining the parameter range in which the algorithm will search for the best candidates: $p_j^{\min} \leq p_j(k) \leq p_j^{\max}$, where k represents the iteration number. Introducing $\bar{p}_j(0) = (p_j^{\min} + p_j^{\max})/2$ and $\sigma_j(0) = (p_j^{\max} - p_j^{\min})/2$, we can compute $\mathbf{X}(0)$ from:

$$X_{ij}(0) = \bar{p}_j(0) + \sigma_j(0)G_{ij}, \quad (14)$$

where G_{ij} is an $N \times N_p$ matrix with random numbers generated from a zero-mean normal distribution with standard deviation of unity.

The next step is to calculate $S_i(0)$ for each set of $\mathbf{x}_i(0)$, ordering them according to increasing values of S_i . Then the first N_{elite} set of parameters is selected, i.e. the N_{elite} -samples with lowest S values, which will be labelled as the elite sample array $\mathbf{X}^{\text{elite}}(0)$.

We then determine the mean and standard deviation of the elite sample, $\bar{p}_j^{\text{elite}}(0)$ and $\sigma_j^{\text{elite}}(0)$ respectively, as:

$$\bar{p}_j^{\text{elite}}(0) = \frac{1}{N_{\text{elite}}} \sum_{i=1}^{N_{\text{elite}}} X_{ij}^{\text{elite}}(0), \quad (15)$$

$$\sigma_j^{\text{elite}}(0) = \sqrt{\frac{1}{(N_{\text{elite}} - 1)} \sum_{i=1}^{N_{\text{elite}}} [X_{ij}^{\text{elite}}(0) - \bar{p}_j^{\text{elite}}(0)]^2}. \quad (16)$$

The array \mathbf{X} at the next iteration is determined as:

$$X_{ij}(1) = \bar{p}_j^{\text{elite}}(0) + \sigma_j^{\text{elite}}(0)G_{ij}, \quad (17)$$

This process is repeated from equation (14), with G_{ij} regenerated at each iteration. The optimization stops when the maximum number of iterations k_{max} is reached.

In order to prevent convergence to a sub-optimal solution due to the intrinsic rapid convergence of the CE method, Kroese, Porotsky & Rubinstein (2006) suggested the implementation of a fixed smoothing scheme for $\bar{p}_j^{\text{elite,s}}(k)$ and $\sigma_j^{\text{elite,s}}(k)$:

$$\bar{p}_j^{\text{elite,s}}(k) = \alpha' \bar{p}_j^{\text{elite}}(k) + (1 - \alpha') \bar{p}_j^{\text{elite}}(k - 1), \quad (18)$$

$$\sigma_j^{\text{elite,s}}(k) = \alpha_d(k) \sigma_j^{\text{elite}}(k) + [1 - \alpha_d(k)] \sigma_j^{\text{elite}}(k - 1), \quad (19)$$

where α' is a smoothing constant parameter ($0 < \alpha' < 1$) and $\alpha_d(k)$ is a dynamic smoothing parameter at k th iteration:

$$\alpha_d(k) = \alpha - \alpha (1 - k^{-1})^q, \quad (20)$$

with $0 < \alpha < 1$ and q is an integer typically between 5 and 10 (Kroese, Porotsky & Rubinstein 2006).

Following Caproni, Monteiro & Abraham (2009), we adopted $\alpha' = 1$, $\alpha = 0.7$ and $q = 5$ throughout this work. In addition, we also assumed $N = 100$, $N_{\text{elite}} = 10$ and $k_{\text{max}} = 800$. It is important to emphasize that this value for k_{max} was chosen so that, independently of the number of CE optimizations that are performed for a fixed $P_{\text{prec,obs}}$ and sense of precession, the remaining precession parameters will always converge to the same numerical value (variations not larger than a few per cent). For the present work, we run our code three times for each particular precession period and sense of precession.

3.3 The merit function S

The merit function $S(k)$ transmits to the CE algorithm the best tentative set of precession parameters at the k th iteration. Following Caproni, Monteiro & Abraham (2009), we have chosen $S(k)$ as:

$$S(k) = \Upsilon(k) + \sum_{i=1}^{N_d} \{ [S_{\alpha_i}(k)]^2 + [S_{\delta_i}(k)]^2 + [S_{r_i}(k)]^2 \}, \quad (21)$$

where:

$$S_{\alpha_i}(k) = \Delta\alpha_i - \Delta\alpha_{\text{mod}_i}(k), \quad (22)$$

$$S_{\delta_i}(k) = \Delta\delta_i - \Delta\delta_{\text{mod}_i}(k), \quad (23)$$

$$S_{r_i}(k) = \Delta r_i - \Delta r_{\text{mod}_i}(k), \quad (24)$$

where $\Delta\alpha_i$ and $\Delta\delta_i$ are, respectively, the right ascension and declination offsets of the jet knot i , $\Delta r_i^2 = \Delta\alpha_i^2 + \Delta\delta_i^2$.

Our code generates, for each observation data t_{obs} , pairs of right ascension and declination offsets based on different values of t_{ej} , which are provided from a given jet-precession

model. The chosen model (RA,Dec)-pair is that which minimizes the square distance between the precession helix and the observed (RA,Dec.) pair, also respecting the condition $t_{\text{obs,ej}} < t_{\text{obs}}$. Therefore, for each observed (RA,Dec.) pair there is always a $t_{\text{obs,ej}}$ that makes $S_{\alpha_i}^2 + S_{\delta_i}^2$ a minimum.

As mentioned in Caproni, Monteiro & Abraham (2009), the terms S_{α_i} and S_{δ_i} strongly constrain the instantaneous jet direction in the optimization process, while inclusion of S_{r_i} provides additional constraint on the modelling of the core-component distances as well as improving the convergence performance of the method.

Jet kinematic modelling performed only on the plane of the sky has an extra potential difficulty: the jet components are not fully independent of each other, in the sense that unique identifications of jet knots also depend on estimates of their individual proper motions. However, identification problems related to fitting procedures, as well as observations poorly sampled in time, may influence the follow-up of the components in time, which consequently might contribute to a misinterpretation of the data. Our CE modelling avoids such potential biases, purely analysing the time behaviour of the sky position of the jet knots without any information concerning previous identification of components. To guarantee that our jet precession modelling will also predict apparent velocities similar to those observed in BL Lacertae, we included a penalty function $\Upsilon(k)$ in the CE optimization process (Caproni, Monteiro & Abraham 2009). Based on independent estimates of the typical apparent velocities of the jet knots in BL Lacertae (e.g., Mutel et al. 1990; Jorstad et al. 2005; Lister et al. 2009), we decided to include in the CE algorithm the following penalty function in equation (21):

$$\Upsilon(k) = \begin{cases} 10, & \text{if } \beta_{\text{obs}}^{\text{min}}(k) < 2 \text{ or } \beta_{\text{obs}}^{\text{max}}(k) > 11, \\ 0, & \text{elsewhere,} \end{cases} \quad (25)$$

where $\beta_{\text{obs}}^{\text{min}}(k)$ and $\beta_{\text{obs}}^{\text{max}}(k)$ are respectively the minimum and maximum values of the apparent jet speeds predicted by a given precession model at iteration k . It is important to emphasize that the choice of $\Upsilon(k) = 10 \text{ mas}^2$ is sufficient to guarantee that any tentative solution providing $\beta_{\text{obs}}^{\text{min}}(k) < 2$ or $\beta_{\text{obs}}^{\text{max}}(k) > 11$ is statistically non-favoured during optimization.

Note that the choice of S is based on the minimization of the quadratic distances between the observational data and those produced by the precession model, while $\Upsilon(k)$ provides extra constraints on the parameters γ and ϕ_0 .

4 THE JET PRECESSION MODEL FOR THE PARSEC-SCALE JET OF BL LACERTAE

4.1 Observational data

The pc-scale jet observational data of BL Lacertae analysed in this work were gathered from the literature (Pearson & Readhead 1988; Charlot 1990; Mutel et al. 1990; Bondi et al. 1996; Gabuzda & Cawthorne 1996; Tateyama et al. 1998; Denn, Mutel & Marscher 2000; Fomalont et al. 2000; Gabuzda & Cawthorne 2003; Stirling et al. 2003; Lister et al. 2009). These data (RA and Dec. offsets) were obtained at frequencies of 5.0, 8.4, 10.7, 15, 24 and 43 GHz, from 1980.93 to 2007.682, providing a

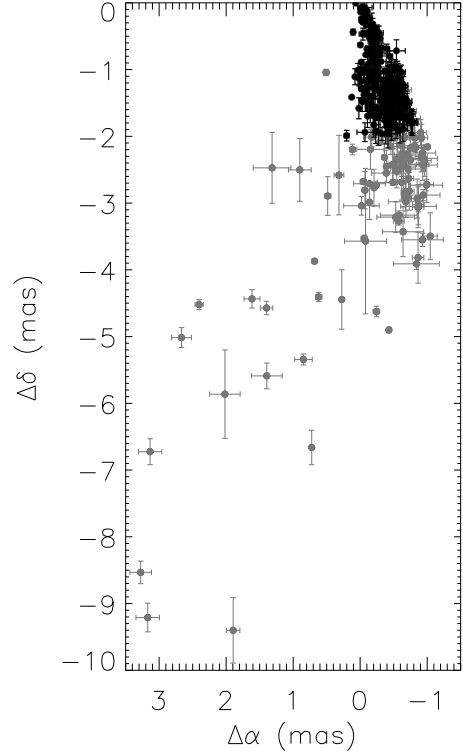


Figure 1. The distribution of right ascension and declination offsets of the jet components of BL Lacertae. Grey circles represent the whole data extracted from the literature, while the black circles are the data analysed by our precession model (core-component distances smaller than 2 mas).

time monitoring of the jet activity in BL Lacertae of about 26.7 yr.

We show in Fig. 1 the corresponding spatial distribution of the jet components of BL Lacertae on the plane of the sky. As already noted in previous papers (e.g., Charlot 1990; Denn, Mutel & Marscher 2000; Stirling et al. 2003), the pc-scale jet of BL Lacertae bends systematically to south-east after a core distance of about 3 or 4 mas, which definitely cannot be addressed exclusively by a jet precession phenomenon. Because of this, we decided to restrict our precession analysis to distances below of 2 mas (see filled circles in Fig. 1), avoiding the bending zone of the jet.

Given the multiwavelength nature of the data used in this work, opacity effects are expected to affect the determination of the absolute core position, which introduce frequency-dependent shifts in the core-component distances and proper motions (e.g., Blandford & Königl 1979; Lobanov 1998; Kovalev et al. 2008). In the case of a precessing jet, these corrections are time-dependent since the angle between the jet and the line-of-sight varies with time (Caproni & Abraham 2004a,b). In the case of BL Lacertae, Mutel et al. (1990) found 0.3 mas for the magnitude of the core-shift between 5.0 and 10.6 GHz. Denn, Mutel & Marscher (2000) estimated a core-component shift between 22 and 43 GHz smaller than 0.1 mas. Croke & Gabuzda (2008) calculated a core shift of 0.20 mas comparing 5.1- and 7.9-GHz maps, while O’Sullivan & Gabuzda (2009), using images at frequencies

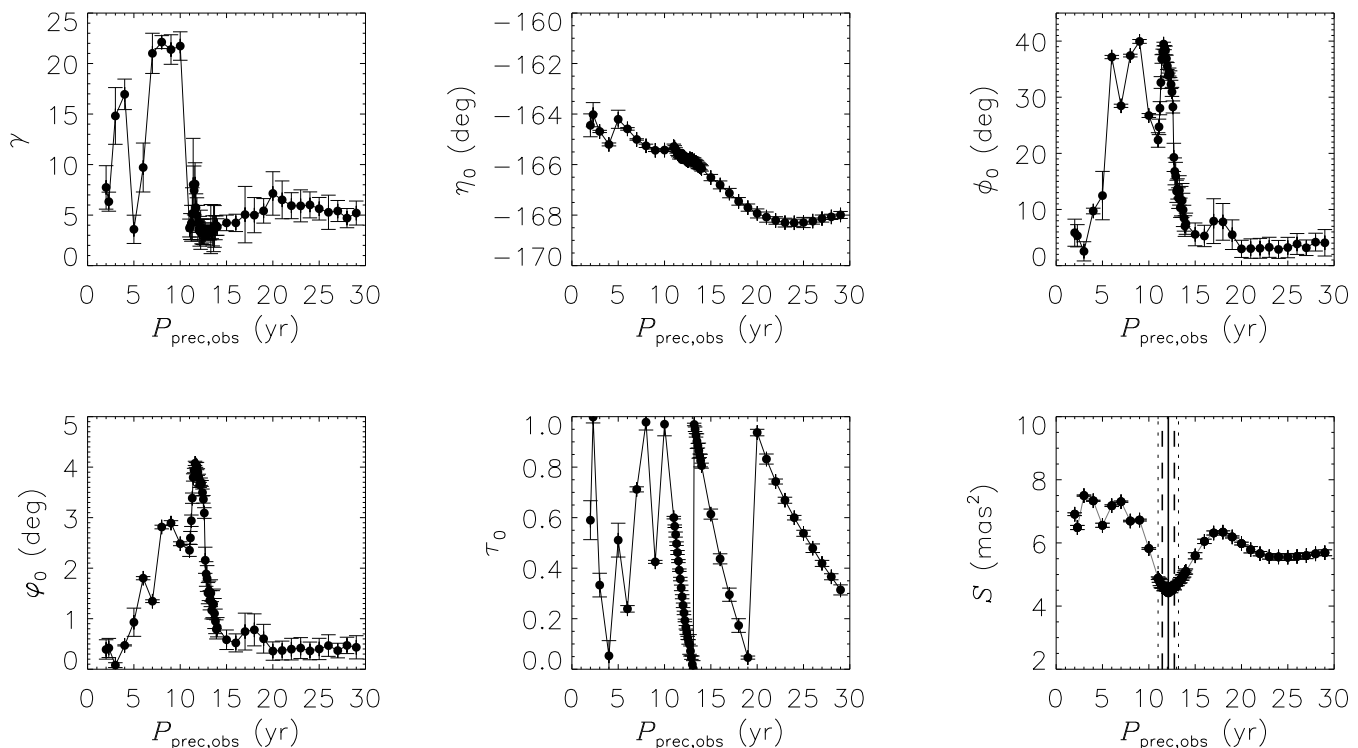


Figure 2. Results for clockwise sense of precession ($\iota = 1$). Dependence of the CE optimized precession model parameters in terms of the observed precession period, as well as the value of the merit function (lower rightmost panel). Steps of 1 yr in precession period were considered, except for the interval between 11 and 14 years, during which differences between consecutive precession periods of 0.1 yr were used. We also included in our analyses the value of 2.29 yr obtained by Stirling et al. (2003). The merit function reaches its minimum at a precession period between 11 and 13.5 yr (dotted vertical lines). The solid and dotted vertical lines mark respectively the weighted mean and standard deviation of the precession period related to the merit-function’s minimum (12.11 ± 0.65 yr).

between 4.6 to 43.1 GHz, found core-shifts values below of 0.43 mas. Considering these works, the mean value of the core-shift in BL Lacertae is roughly 0.2 mas, which will not influence significantly our jet precession modelling given the intrinsic uncertainties of the data, as well as the high fraction of 15-GHz data in our sample¹. Because of that, we will hereafter neglect core opacity effect in our jet precession analyses.

4.2 Estimating the precession period and the sense of precession of the BL Lacertae jet

The precession period and the sense of precession are quantities not automatically optimized by our CE method. Thus, some extra procedure is necessary to determine those parameters. Following Caproni, Monteiro & Abraham (2009),

¹ We run additional CE optimizations considering two subsets of the original data to verify quantitatively this claim. The two subsets correspond to 15-GHz and 15+43 GHz data (about 44 and 83 per cent of the original data set, respectively). For 15-GHz data, typical changes in the values of the precession parameters in relation to our best model (see Table 1 in Section 4.4) are usually less than ~ 7 per cent (not exceeding ~ 25 per cent). For 15+43 GHz data, the typical differences are less than ~ 3 per cent (~ 15 per cent in the worst case). The decrease in those values is a consequence of the increase of the time coverage of 15+43 GHz data (from ~ 8.3 yr to ~ 13 yr).

we mapped the dependence of the jet-precession model fitting with the precession period and the sense of precession. We varied the value of the precession period measured in the observer’s reference frame from 2 to 30 yr in steps of 1 yr for both clockwise and counterclockwise senses of precession, covering those values previously suggested in the literature (Stirling et al. 2003; Tateyama 2009). An extra refinement step of 0.1 yr was adopted between 11 and 14 yr, in which the merit function presented a minimum, as will be discussed later.

For each tentative precession period, our CE method searched for the best set of precession model parameters in the ranges: $0.95 \leq \beta \leq 0.999$ ($3.2 \leq \gamma \leq 22.4$), $-180^\circ \leq \eta_0 \leq -150^\circ$, $0.1 \leq \phi_0 \leq 40^\circ$, $0^\circ \leq \varphi_0 \leq 30^\circ$ and $0 \leq \tau_{0,s} \leq 1$. It is important to emphasize that these parameter ranges contain the jet parameter values for BL Lacertae derived in previous works (e.g., Mutel et al. 1990; Denn, Mutel & Marscher 2000; Stirling et al. 2003; Tateyama 2009). Note also that the hypothesis of a non-precessing jet is incorporated in our analysis, since $\varphi_0 = 0^\circ$ is one of the possibilities to fit the observational data.

We show in Figs. 2 and 3 the optimized precession model parameters and the merit function versus the precession period in the observer’s reference frame, for clockwise and counterclockwise senses of precession, respectively. Among all precession model parameters, η_0 exhibits the smallest variation in terms of $P_{\text{prec,obs}}$ (only about 4°). Extreme values for γ and ϕ_0 were found for some tentative

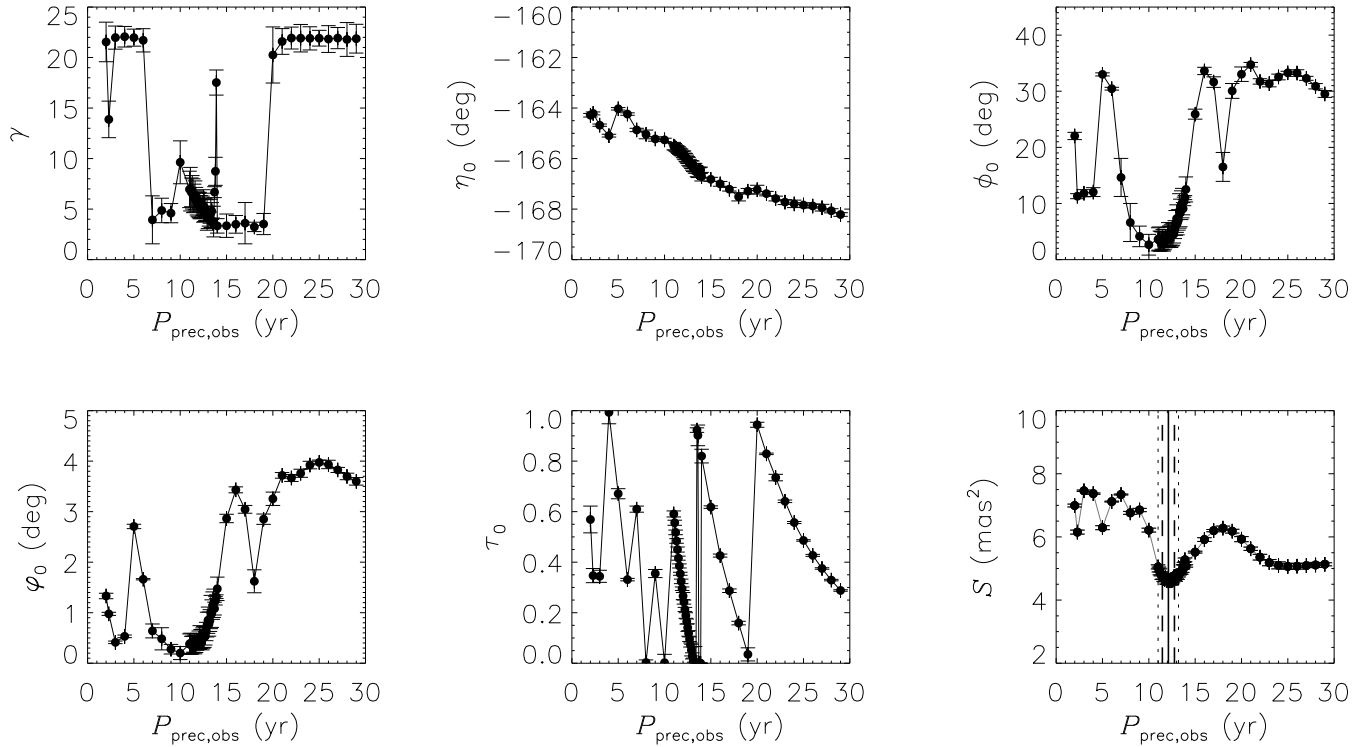


Figure 3. Results for counterclockwise sense of precession ($\iota = -1$). Dependence of the CE optimized precession model parameters in terms of the observed precession period, as well as the value of the merit function (lower rightmost panel). Steps of 1 yr in precession period were considered, except for the interval between 11 and 14 years, during which differences between consecutive precession periods of 0.1 yr were used. We also included in our analyses the value of 2.29 yr obtained by Stirling et al. (2003). The merit function reaches its minimum at a precession period between 11 and 13.5 yr (dotted vertical lines). The solid and dotted vertical lines mark respectively the weighted mean and standard deviation of the precession period related to the merit-function’s minimum (12.11 ± 0.65 yr).

precession periods; they correspond to $5 < P_{\text{prec,obs}} < 14$ for clockwise precession, and $P_{\text{prec,obs}} < 5$ or $P_{\text{prec,obs}} > 19$ for counterclockwise precession.

A well-defined minimum for the merit function is found at a precession period of about 12.1 years, independently of the sense of precession. The values of both minima are practically identical ($S = 4.511 \pm 0.109 \text{ mas}^2$ and $S = 4.606 \pm 0.072 \text{ mas}^2$ for clockwise and counterclockwise precession, respectively), making impossible to obtain information about the sense of precession from the merit function alone. The difficulty in detecting the correct sense of precession was also found by Stirling et al. (2003). As mentioned by them, the problem probably resides on the lack of observational data with larger core-component distances employed in the modelling. However, other constrains on the optimized precession parameters can be used instead, namely the interval of observed superluminal velocities, the boosting parameter, which depends on the Doppler factor, and the jet-to-counterjet flux density ratio Ξ , which should be large enough to guarantee that the counterjet is not observed. This last quantity can be calculated from:

$$\Xi(\tau_s) = \left[\frac{1 + \beta \cos \phi(\tau_s)}{1 - \beta \cos \phi(\tau_s)} \right]^{p+\alpha}, \quad (26)$$

where p is equal to 2 or 3 for a continuous or clumpy jet, respectively (e.g., Lind & Blandford 1985), and α is the spectral index of the flux density distribution in terms of the observed frequency ν ($S_\nu \propto \nu^{-\alpha}$).

We plotted the dependency of the interval of predicted superluminal velocities, Doppler factor and jet-counterjet ratio as a function of the precession period in the observer’s reference frame in Figs. 4 (clockwise sense of precession) and 5 (counterclockwise sense). Looking carefully at $P_{\text{prec,obs}} \sim 12.1$ yr we can see that the clockwise jet-precession model predicts too low value of Ξ (~ 300), which implies the possibility of counterjet detection in interferometric radio images, given their typical dynamic ranges. However, such detection has never been achieved, which indicates that a clockwise jet-precession scenario is not appropriated for BL Lacertae. On the other hand, the counterclockwise jet-precession model predicts $\Xi \sim 3.5 \times 10^5$, in agreement with available observational data.

In addition, our counterclockwise precession model predicts Doppler-boosting factor ranging from 8.8 and 9.4 (in contrast to the clockwise model that predicts a variation between 1.2 and 1.7), in good agreement with independent estimates of the Doppler-boosting parameter for BL Lacertae found in the literature that suggest $\delta \gtrsim 7$ (e.g., Jorstad et al. 2005; Hovatta et al. 2009; Wu et al. 2011). Therefore, the counterclockwise 12.1-yr jet precession scenario is favoured in the case of BL Lacertae.

The 12.1-precession period found in this present work is not in agreement with the precession periods of 2.29 and 26.0 years reported previously by Stirling et al. (2003) and Tateyama (2009), respectively. However, Mutel & Denn (2005), analysing a different set of 43-GHz images (includ-

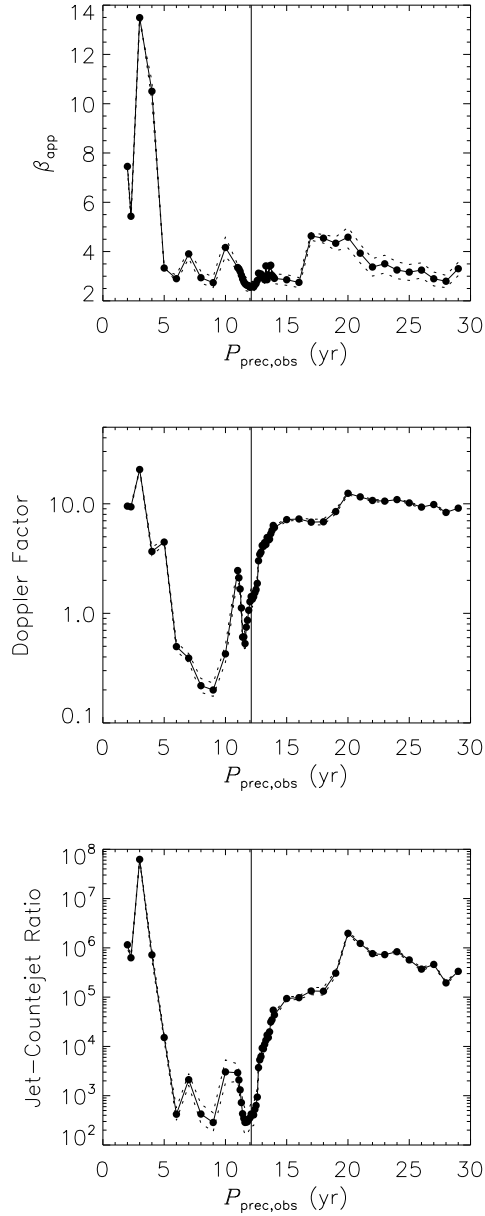


Figure 4. Results for clockwise sense of precession ($\iota = 1$). Apparent velocity, Doppler-boosting factor and jet-counterjet ratio (assuming $p = 2$ and $\alpha = 0.8$) predicted by our CE optimized model as a function of the precession period. Full circles represent those quantities calculated at $\phi = \phi_0$, while the dotted lines show their respective upper and lower limits allowed by the precession model. The solid vertical line marks the favoured precession period of 12.1 yr.

ing some overlapping epochs with Stirling et al. 2003), concluded that changes in the structural position angle² of the radio core of BL Lacertae could present a periodicity of 12.1 yr, as statistically significant as that of 2.29 yr. Note that all these previous works analysed a substantially shorter interval of observations (~ 3.1 years in Stirling et al. 2003, ~ 5.1

² Angle defined by the relative orientation between components C1 and C2 detected in the 43-GHz VLBI images of BL Lacertae (see Stirling et al. 2003).

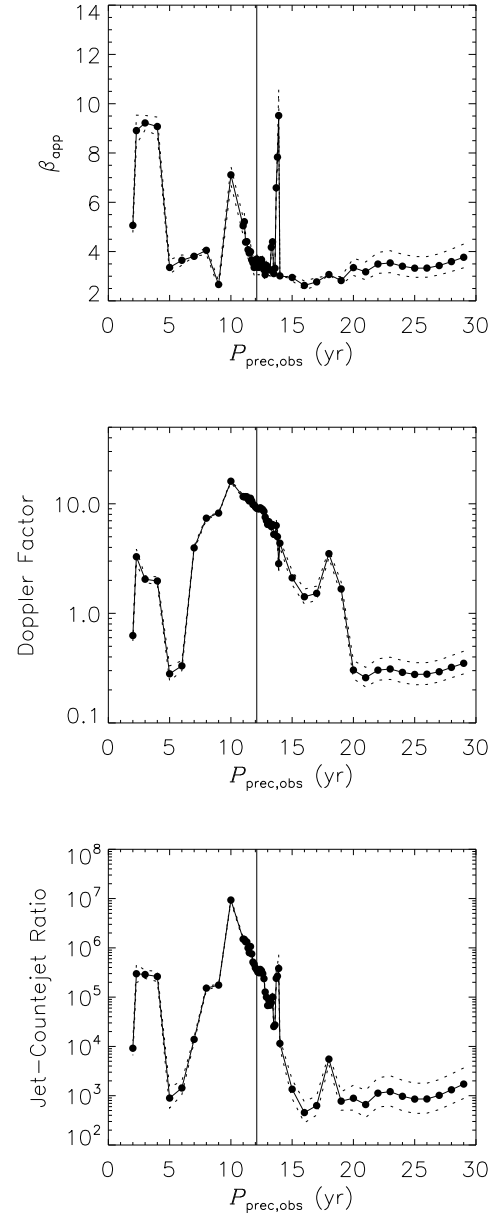


Figure 5. Results for counterclockwise sense of precession ($\iota = -1$). Apparent velocity, Doppler-boosting factor and jet-counterjet ratio (assuming $p = 2$ and $\alpha = 0.8$) predicted by our CE optimized model as a function of the precession period. Full circles represent those quantities calculated at $\phi = \phi_0$, while the dotted lines show their respective upper and lower limits allowed by the precession model. The solid vertical line marks the favoured precession period of 12.1 yr.

years in Mutel & Denn 2005 and ~ 12 yr in Tateyama 2009) in comparison to this present work (~ 26.7 yr), which might be responsible for such discrepancies. Another possibility is that the 2.29-yr period is related to some extra phenomenon, such as nodding modulation of the precession angle, for instance (see Section 6 for a more detailed discussion about this possibility).

4.3 The non-precessing jet scenario

As mentioned before, the non-precessing jet hypothesis ($\varphi_0 = 0^\circ$) was also checked by our CE technique during each optimization processes. Even though the validation tests (Caproni, Monteiro & Abraham 2009) showed that the technique is able to determine whether precession is taking place, we decided to perform an independent model optimization, forcing $\varphi_0 = 0^\circ$, and rerun the code to optimize the remaining jet model parameters. We found that the value of merit function (defined by equation 21) in this situation corresponds to $\sim 7.8 \text{ mas}^2$, at least 1.5 times larger than that found for $P_{\text{prec,obs}} \sim 12.1$ yr. To estimate the statistical significance of such difference, we applied the non-parametric two-sample two-dimensional Kolmogorov–Smirnov test, (2DKS test hereafter: see e.g., Peacock 1983; Fasano & Franceschini 1987; Press et al. 1997).

In brief, this test compares two-dimensional data sets in terms of the maximum cumulative difference between them, measuring the probability of these two data sets being drawn from the same parent distribution. In this work, the data sets are the observed and model predicted jet-knot position offsets from the core, so that comparison is made using pairs of $(\Delta\alpha_{\text{obs}_i}, \Delta\delta_{\text{obs}_i})$ and $(\Delta\alpha_{\text{mod}_i}, \Delta\delta_{\text{mod}_i})$, the i th data point of the respective data sets. Note that these two samples are not strictly independent since the model coordinates are calculated from a model that was constrained, on the other hand, from the observed positions of the jet knots. Although it is in contradiction to the underlying hypothesis of independence of the two analysed data sets, Wild et al. (2005) argue if the number of the observed data points is much greater than the number of the model parameters, such effect should be small enough to allow the application of the 2DKS test. This requirement is fulfilled in our data sets.

Unfortunately, another potential drawback concerning the multidimensional generalization of the Kolmogorov–Smirnov test is related to the calculation of the maximum cumulative difference in two or more dimensions, which is not uniquely defined (e.g., Peacock 1983; Fasano & Franceschini 1987; Press et al. 1997). It introduces a possible dependency in the determination of the maximum cumulative difference with the shape of the parent two-dimensional probability distribution. However, Fasano & Franceschini (1987) showed from Monte Carlo simulations that their parametrisation for 2DKS test is distribution-free in good approximation. In any case, the resulting probabilities obtained from 2DKS tests are not as rigorously reliable as in the one-dimensional case, so that they must be interpreted warily (e.g., Press et al. 1997).

The application of the 2DKS test for our counterclockwise 12.1-yr jet precession model leads to a probability of ~ 15 per cent. As suggested in Press et al. (1997) and Wild et al. (2005), a 2DKS probability above ~ 10 –20 per cent can be used to claim reasonable agreement between the two analysed data sets. Conversely, this probability drops to 0.028 per cent for the non-precessing jet scenario. Thus, the 2DKS tests indicate that the probability of the observed and model data sets being drawn from the same parent distribution is 15 per cent for our best precession model, but less than 0.1 per cent for the non-precession scenario. This demonstrates that our model provides a significantly bet-

Table 1. The best precession model parameters optimized by our CE algorithm for a counterclockwise sense of precession ($\iota = -1$). The uncertainties in each parameter correspond to 1σ level.

$P_{\text{prec,obs}}$ (yr)	12.11 ± 0.65
$P_{\text{prec,s}}$ (yr)	550 ± 247
β	0.9824 ± 0.0087
γ	5.35 ± 1.31
η_0 (deg)	-165.86 ± 0.16
ϕ_0 (deg)	4.43 ± 2.16
φ_0 (deg)	0.51 ± 0.24
$\tau_{0,s}$	0.242 ± 0.008

ter description of the collected observations for BL Lacertae than a non-precessing model, although some discrepancies between our best model and observational data still remain.

4.4 Model parameters for 12.1-years counterclockwise precession period

As presented in last section, the precession of the pc-scale jet of BL Lacertae occurs in a counterclockwise sense, respecting a periodicity of about 12.1 yr in the observer’s reference frame. The CE optimized precession model parameters related to this period are given in Table 1. Precession-model parameters and their respective uncertainties were estimated following Caproni et al. (2011) (equations 10 and 11 in their paper). Note that the precession rate in the source’s reference frame is substantially slower, as expected from relativistic effects (see equation 11).

Comparison between snapshots of the precession helix generated from the parameters listed in Table 1 and the right ascension and declination offsets of the observed jet knots of BL Lacertae can be visualized in the section entitled Supporting Information, published in the online version of this work. The distribution of the residuals in right ascension and declination directions (generated from the difference between the model-predicted and observed positions of jet knots) is compatible with zero-mean value in both directions. Their associated root mean square values (rms) are ~ 0.12 and ~ 0.03 mas in right ascension and declination directions, respectively. It strongly indicates that the mean jet position angle predicted from our best model is quite well determined.

Applying the same analysis for a non-precessing jet, it is possible to note an increase of the spread of the residuals in relation to that found from our best precession model. It is quantitatively corroborated by the slight increase of the rms in both directions (~ 0.15 mas in right ascension and ~ 0.04 mas in declination), reinforcing our conclusion that the non-precessing jet scenario is not suitable for BL Lacertae. In relation to the previously published precession models by Stirling et al. (2003) and Tateyama (2009), the amplitude of residuals is even higher in comparison with a non-precessing jet scenario and our best precession model. Indeed, this was already expected given their larger values of S ($\sim 17 \text{ mas}^2$ for Stirling et al. 2003 and 15 mas^2 for Tateyama 2009, much higher than our own value for non-precession case).³

³ In order to compare the merit function of our best jet-precession

According to our precession model, the expected apparent velocities of the jet of BL Lacertae are always superluminal, ranging from about 3.4 to 4.0c. Components having such velocities have been observed in previous works (e.g., Mutel et al. 1990; Jorstad et al. 2005; Gabuzda & Cawthorne 2003; Lister et al. 2009), even though some quasi-stationary components ($\beta_{\text{obs}} \ll 1$), as well as faster knots have been also detected in BL Lacertae (e.g., Jorstad et al. 2005; Lister et al. 2009). It should not be interpreted as a serious problem of our model since some jet components of BL Lacertae exhibit non-ballistic trajectories, which is not taken into account in our present parametrization. Indeed, the theory of linear perturbations, as well as numerical simulations, has shown that jet precession can induce instabilities in the jet flow (Hardee 2000, 2001, 2002). The observational counterparts of these jet instabilities may be seen as non-ballistic knots in VLBI images. Therefore, the scenario adopted in this work (ballistic motions plus jet precession) does not exclude the existence of helical motions in the jet of BL Lacertae. Note also that our predicted apparent velocities are different from those found by Stirling et al. (2003) ($\beta_{\text{obs}} \sim 6.7$) and Tateyama (2009) ($7 < \beta_{\text{obs}} < 10$).

Because of precession, jet viewing angle varies approximately between 4° and 5° , which is in reasonable agreement with the values derived from the characteristics of the variability in the multiwavelength light curves of BL Lacertae (Hovatta et al. 2009; Raiteri et al. 2010; Savolainen et al. 2010; Wu et al. 2011). The predicted jet viewing angles from our precession model are between those found by Stirling et al. (2003) ($6^\circ < \phi < 12^\circ$) and Tateyama (2009) ($1.5^\circ < \phi < 3^\circ$).

The jet inlet position angle on the plane of the sky ranges from -172° to -159° , providing a total variation of $\sim 13^\circ$ which is approximately half of those obtained by Stirling et al. (2003) and Tateyama (2009). This angular amplitude means an amplitude variation of 0.46 mas at 2 mas from the core, which is about twelve and four times greater than typical observational uncertainties in the right ascension and declination positions of the jet components, respectively.

As mentioned previously, the Doppler-boosting parameter varies roughly from 8.8 to 9.4 in our model, which means that the jet-counterjet flux ratio ranges from 3.3×10^5 to 3.9×10^5 (considering a continuous jet with a spectral index of 0.8; e.g., Lind & Blandford 1985), implying in a non-detected counterjet at pc scales. This result also supports the hypothesis claimed by Stirling et al. (2003) that component C1 is not the manifestation of the counterjet.

The observational data used to constrain our optimized precession model covers 26.7 yr of monitoring, which means an interval of about 2.2 times longer than the estimated

precession period of 12.1 yr. At this point it is important to emphasize that our CE model technique is able to deal properly with short time samplings, as can be seen in the validation tests published in Caproni, Monteiro & Abraham (2009). One of these tests employed synthetic data formed by no more than 50 sky positions (about one sixth of the data analysed in this work) and covered only 1.5 precession periods. Therefore, this strongly suggests that our results are not influenced by the relatively short time covering of the data in terms of the 12.1-yr precession period.

5 THE UNDERLYING JET OF BL LACERTAE

The jet precession period of 12.1 yr has no counterpart detected in analyses of the historical light curves of BL Lacertae conducted up to now. Quasi-periodic variations in the radio light curves of BL Lacertae have been reported in the literature, ranging roughly from 0.7 to 8 yr depending on the frequency and time coverage of the observations (Kelly et al. 2003; Villata et al. 2004). In optical domains the situation is almost the same: there is some evidence of a periodicity of about 7-8 yr but this is still inconclusive (Hagen-Thorn et al. 1997; Villata et al. 2004). Similarly, Fan et al. (1998) reported a strong signature of a periodicity of 13.97 yr in the B-band light curve, as well as shorter periods of 0.66 and 0.88 yr, also found by Webb et al. (1988).

Although some works have shown the viability of jet precession in producing detectable signatures in the light curves of some sources (e.g., Caproni & Abraham 2004a,b), it should not be expected for all precessing objects. As mentioned by Mutel & Denn (2005), the main contribution to the observed flux of BL Lacertae may be due to the extended jet, which is not varying its orientation and consequently may be masking any precession signature. Another possibility that cannot be excluded is that the underlying jet is intrinsically weak, so that even Doppler-boosting effects modulated by precession are not sufficiently strong to make its contribution detectable.

We compared the historical 8.4-GHz and B band⁴ light curves with upper limits for the observed flux density of the underlying jet⁵ predicted from our best model. We assumed simplistically that the intrinsic flux density of the underlying jet S_s did not vary along the observation time, following the relation $S_{\text{obs}}(t_{\text{obs}}) = S_s[\delta(t_{\text{obs}})]^{2+\alpha}$ (similarly to Caproni & Abraham 2004b). We assumed $\alpha \sim 0.0$ for the radio regime (Denn, Mutel & Marscher 2000) and $\alpha = 2.0$ for the optical band (Brown et al. 1989). To keep the underlying jet contribution always below the measured total flux densities, S_s must be lower than 18 mJy and 0.30 μ Jy at radio and optical frequencies, respectively.

The small variation in the value of the Doppler-boosting factor (between ~ 8.8 and 9.4) implies a small variation in

model quantitatively with those derived by Stirling et al. (2003) and Tateyama (2009), we generated precession helices based on the values of the parameters determined by those authors and compared them with the same observational data used in our work. Thus, these comparisons respect the same conditions used in this work (e.g. penalty function, jet region, frequency range, etc.), as well as their related small 2DKS test probabilities (0.039 per cent for Stirling et al. 2003 and 1.6×10^{-4} per cent for Tateyama 2009).

⁴ Based on data taken and assembled by the WEBT collaboration and stored in the WEBT archive at the Osservatorio Astronomico di Torino - INAF (<http://www.oato.inaf.it/blazars/webt/>).

⁵ The term underlying jet refers to a continuous or quasi-continuous distribution of plasma elements in the jet in which shocks and/or plasmons (jet components) propagate (in a similar sense as given by Lind & Blandford 1985).

the amplitude of the observed flux density of the underlying jet (between ~ 0.18 and 0.23 mJy in the B band and from about 1.39 and 1.59 Jy at 8.4 GHz). We speculate that it might be the reason for the non-detection of such 12.1 yr periodicity from the previous statistical analyses of the light curves of BL Lacertae. Notwithstanding, the underlying jet contribution might be responsible for a plateau-like structure (with mean values of about 0.21 mJy in the B band and 1.49 Jy at 8.4 GHz) underneath of the main flux variations of BL Lacertae, which are probably produced by the jet components themselves; this can be interpreted as either shocks moving down the jet (e.g., Blandford & Königl 1979; Hughes, Aller & Aller 1985, 1989) or plasmoids ejected from the core (e.g., Pauliny-Toth & Kellermann 1966).

6 JET PRECESSION AND NODDING MOTIONS IN BL LACERTAE

Stirling et al. (2003) analysed the structural position angle defined by the relative orientation between components C1 and C2, as well as the polarization angle in radio and optical observations, finding a periodic modulation of 2.29 yr in both quantities. They interpreted those results as due to the precession of the jet inlet region. We explore in this section an alternative interpretation for this short period in terms of a nutation motion produced in a supermassive binary black hole system.

Katz et al. (1982) established the relation between the characteristics of a precessing accretion disc in close binary systems and the frequency ω_n of short-term nodding motions:

$$\omega_n = 2(\omega_{\text{orb}} - \omega_s), \quad (27)$$

where ω_{orb} is the orbital angular velocity of the secondary black hole. Note that ω_s should be negative since the induced precession is retrograde, in the sense of being contrary to the rotation of the accretion disk (eg., Katz et al. 1982).

Assuming that the nodding oscillation has a period of 2.29 yr in the observer's reference frame, we can use equation (27) to calculate the value of the orbital period of the secondary black hole $P_{\text{orb,obs}}$ to produce the inferred 12.1 -yr precession period. It implies $P_{\text{orb,obs}} = 7.4 \pm 1.8$ yr or $P_{\text{orb,s}} = 335 \pm 173$ yr in the source's reference frame, the respective uncertainties having been obtained from error propagation of the involved periods.

From the $P_{\text{orb,s}}$, we can derive the distance between the two black holes R_{ps} from the Kepler's third law:

$$R_{\text{ps}}^3 = \frac{GM_{\text{tot}}}{4\pi^2} P_{\text{orb,s}}^2, \quad (28)$$

where G is the gravitational constant, and $M_{\text{tot}} = M_{\text{p}} + M_{\text{s}}$, the sum of the masses of the primary and secondary black holes, respectively.

Several works have attempted to estimate the mass of the supermassive black hole in BL Lacertae (Fan, Xie & Bacon 1999; Wu & Urry 2002; Marconi & Hunt 2003; Ghisellini et al. 2010; Capetti, Raiteri & Buttiglione 2010), which seems to have about $1.5 - 6 \times 10^8 M_{\odot}$. Assuming that M_{tot} corresponds to the mean value of those estimates, i.e. $M_{\text{tot}} = 3.75 \times 10^8 M_{\odot}$, we calculated the distance between the black holes

from equation (28), providing $R_{\text{ps}} = 0.17 \pm 0.07$ pc, which corresponds to ~ 0.13 mas at the distance of BL Lacertae.

To put a lower limit for the ratio between the masses of the secondary and primary black holes, $q = M_{\text{s}}/M_{\text{p}}$, it is necessary to verify in which conditions the orbital period of the secondary can produce the inferred accretion disc/jet precession rate. Assuming that jet precession of BL Lacertae is induced by torques in the primary accretion disc due to a non-coplanar secondary black hole (e.g., Katz 1997; Papaloizou & Terquem 1995; Larwood 1997; Romero et al. 2000; Caproni & Abraham 2004a,b; Caproni et al. 2006), and taking $R_{\text{prec}} \leq R_{\text{out}}$ (Romero et al. 2000), where R_{prec} and R_{out} are respectively the outer radii of the precessing part of the disc and the disc itself, we can write (Caproni et al. 2006):

$$\left(\frac{|P_{\text{prec,s}}|}{P_{\text{orb,s}}} \right) \cos \varphi_0 \geq \frac{4}{3} \left(\frac{5-n}{7-2n} \right) \left[\frac{(1+q)^{1/3}}{0.88q^{2/3}f(q)} \right]^{3/2}, \quad (29)$$

where n is the polytropic index of the gas (e.g., $n = 3/2$ for a non-relativistic gas and $n = 3$ for the relativistic case), and the function $f(q)$ has the form (Eggleton 1983):

$$f(q) = \frac{0.49q^{2/3}}{0.6q^{2/3} + \ln(1+q^{1/3})}. \quad (30)$$

The value of the left-hand of equation (29) is completely defined by our precession and nutation models, while the right-hand of the same equation depends only on the parameter q . Assuming $n = 3/2$, equation (29) is satisfied only if $q \gtrsim 5.75$, which implies $M_{\text{p}} \lesssim 5.5 \times 10^7 M_{\odot}$ and $M_{\text{s}} \gtrsim 3.2 \times 10^8 M_{\odot}$. It is important to emphasize that there is no problem concerning secondary black hole to be more massive than primary one. The word primary in our context only means that the observed jet is generated from the primary black hole. It is not new at all, since some previous papers had already claimed systems with more massive secondary black hole than primary ones (e.g., Romero et al. 2000; Britzen et al. 2001).

The time stability of such system can be verified by calculating the timescale τ_{GW} for losses due to gravitational radiation from the expression (Begelman, Blandford & Rees 1980; Shapiro & Teukolsky 1983):

$$\tau_{\text{GW}} = \frac{5c^5}{256} \frac{r_{\text{ps}}^4}{(GM_{\text{tot}})^3} \frac{(1+q)^2}{q}, \quad (31)$$

which is minimized when $q = 1$.

For the supermassive binary black hole system considered in this work, we have $\tau_{\text{GW}} \geq 70$ Gyr, which is much longer than the age of the Universe. This indicates no significant changes in the orbit of the secondary and consequently to jet precession rate during the interval of the observations used in this work.

Concerning the intrinsic amplitude of the nutation motion, our calculation based on equation (4) in Katz (1997) leads to a value of about $0^\circ.10$. Its inclusion into our jet-precession model generates an additional amplitude variation at the position angle of the jet on the plane of sky of about $\pm 2^\circ.5$, which may be detected in the millimetre data, in principle.

We can see that a putative supermassive binary black hole system with the physical characteristics described above can drive not only the jet-precession period found in

this work, but also a nutation with a period of 2.29 yr, which might be responsible for variations in the structural position angle of the pc-scale radio core, as well as in the polarization angles reported by Stirling et al. (2003) and Mutel & Denn (2005).

7 CONCLUSIONS

Stirling et al. (2003) and Tateyama (2009) have claimed the existence of precession motions in the pc-scale jet of BL Lacertae of 2.29 and 26 yr, respectively. In this work we revisited this issue, investigating temporal changes of the observed right ascension and declination offsets of the jet knots in terms of our relativistic jet-precession model.

Our precession model is characterized by seven parameters: precession period, jet bulk velocity, aperture angle of the precession cone, the angle between the cone axis and the line of sight, position angle of the cone axis on the plane of the sky, sense of precession, and precession angular phase. These parameters were optimized via heuristic cross-entropy (CE) method, comparing the projected precession helix with the two-dimensional position of the jet components on the plane of the sky, following Caproni, Monteiro & Abraham (2009). The search for the best precession model for BL Lacertae is performed considering parameter ranges that contain the jet parameter values derived in previous works (e.g., Mutel et al. 1990; Denn, Mutel & Marscher 2000; Stirling et al. 2003; Tateyama 2009), as well as the case of a non-precessing jet ($\varphi_0 = 0^\circ$).

Our optimized best model is compatible with a jet having a bulk velocity of 0.9824c, which is precessing in a counterclockwise sense with a period of about 12.1 yr at the observer's reference frame (~ 550 yr at the source's referential framework), and changing its orientation in relation to the line of sight between approximately $3^\circ 9'$ and $4^\circ 9'$. The position angle of the precession cone axis on the plane of the sky is about -166° . It is important to emphasize that these precession parameters lead to $S \approx 4.6 \text{ mas}^2$, which is significantly lower than the values obtained for both a non-precessing model and the previously published precession models.

Searches for periodic variation in the historical light curves of BL Lacertae have not revealed any signature of flux variability occurring at a periodicity of 12.1 yr (e.g., Webb et al. 1988; Fan et al. 1998; Hagen-Thorn et al. 1997; Kelly et al. 2003; Villata et al. 2004). We speculate that the non-detection of the periodicity of 12.1 yr might be attributed to small variations in the amplitude of the Doppler-boosting factor predicted by our model, which implies small variations of the observed flux density associated to the underlying jet. Nevertheless, the underlying jet contribution might be responsible for a plateau-like structure underneath of the main flux variations of BL Lacertae.

Assuming that jet precession has its origin in a supermassive binary black hole system, we show that the 2.3-yr periodic variation in the structural position angle of the VLBI core of BL Lacertae reported by Stirling et al. is compatible with a nutation phenomenon if $q \gtrsim 5.75$. The orbital period of the secondary black hole at the source's reference

frame is approximately 335 yr, which means a distance between primary and secondary black holes of about 0.17 pc.

Further monitoring of the pc-scale activity of BL Lacertae is necessary to confirm the validity of our precession model, as well as the supermassive binary black hole scenario proposed in this work.

ACKNOWLEDGMENTS

This work was supported by the Brazilian agencies Fundação de Amparo à Pesquisa do Estado de São Paulo (FAPESP) and Conselho Nacional de Desenvolvimento Científico e Tecnológico (CNPq). We thank Dr Massimo Villata for making available the WEBT *B*-band photometric data of BL Lacertae used in this work. This research has also made use of data, kindly provided by Dr Margo Aller from the University of Michigan Radio Astronomy Observatory, which has been supported by the University of Michigan and by a series of grants from the National Science Foundation, most recently AST-0607523, as well as NASA Fermi grants NNX09AU16G, NNX10AP16G, and NNX11AO13G. We also thank the anonymous referee for a detailed and careful report that improved substantially the presentation of this work.

REFERENCES

- Antonucci, R. R. J. 1986, *ApJ*, 304, 634
- Begelman, M. C., Blandford, R. D., Rees, M. J. 1980, *Nature*, 287, 307.
- Blandford, R. D., Königl, A. 1979, *ApJ*, 232, 34
- Bondi, M., Padrielli, L., Fanti, R., Ficarra, A., Gregorini, L., Mantovani, F., Bartel, N., Romney, J. D., et al. 1996, *A&A*, 308, 415
- Britzen, S., Roland, J., Laskar, J., Kokkotas, K., Campbell, R. M., Witzel, A. 2001, *A&A*, 374, 784
- Brown, L. M. J. et al. 1989, *ApJ*, 340, 129
- Capetti, A., Raiteri, C. M., Buttiglione, S. 2010, *A&A*, 516, 59
- Caproni, A., Abraham, Z. 2004a, *ApJ*, 602, 625
- Caproni, A., Abraham, Z. 2004b, *MNRAS*, 349, 1218
- Caproni, A., Livio, M., Abraham, Z., Mosquera Cuesta, H. J. 2006, *ApJ*, 653, 112
- Caproni, A., Monteiro, H. Abraham, Z. 2009, *MNRAS*, 399, 1415
- Caproni, A., Monteiro, H. Abraham, Z., Teixeira, D. M., Toffoli, R. T. 2011, *ApJ*, 736, 68
- Charlot, P. 1990, *A&A*, 229, 51
- Croke, S. M., Gabuzda, D. C. 2008, *MNRAS*, 386, 619
- de Boer, P. -T., Kroese, D. P., Mannor, S., Rubinstein, R. Y. 2005, *Annals of Operations Research*, 134, 19.
- Denn, G. R., Mutel, R. L., Marscher, A. P. 2000, *ApJS*, 129, 61
- Eggleton, P. P. 1983, *MNRAS*, 204, 449
- Fan, J. H., Xie, G. Z., Pecontal, E., Pecontal, A., Copin, Y. 1998, *ApJ*, 507, 173
- Fan, J. H., Xie, G. Z., Bacon, R. 1999, *A&AS*, 136, 13
- Fasano, G., Franceschini, A. 1987, *MNRAS*, 225, 155
- Fomalont, E. B., Frey, S., Paragi, Z., Gurvits, L. I., Scott,

- W. K., Taylor, A. R., Edwards, P. G., Hirabayashi, H. 2000, *ApJS*, 131, 95
- Gabuzda, D. C., Cawthorne, T. V. 1996, *MNRAS*, 283, 759
- Gabuzda, D. C., Cawthorne, T. V. 2003, *MNRAS*, 338, 312
- Ghisellini, G., Tavecchio, F., Foschini, L., Ghirlanda, G., Maraschi, L., Celotti, A. 2010, *MNRAS*, 402, 497
- Gower, A. C., Gregory, P. C., Hutchings, J. B., Unruh, W. G. 1982, *ApJ*, 262, 478
- Hagen-Thorn, V. A., Marchenko, S. G., Mikolaichuk, O. V., Yakovleva, V. A. 1997, *Astron. Rep.*, 41, 154
- Hardee, P. E. 2000, *ApJ*, 533, 176
- Hardee, P. E. 2001, *ApJ*, 555, 744
- Hardee, P. E. 2002, *New Astron. Rev.*, 46, 427
- Hovatta, T., Valtaoja, E., Tornikoski, M., Lhteenmki, A. 2009, *A&A*, 494, 527.
- Hyvönen, T., Kotilainen J. K., Falomo R., Örndahl E., Pursimo, T. 2007, *A&A*, 476, 723
- Jorstad, S. G., et al. 2005, *AJ*, 130, 1418
- Hughes, P. A., Aller, H. D., Aller, M. F. 1985, *ApJ*, 289, 301
- Hughes, P. A., Aller, H. D., Aller, M. F. 1985, *ApJ*, 341, 68
- Katz, J. I., Anderson, S. F., Margon B., Grandi, S. A. 1982, *ApJ*, 260, 780
- Katz, J. I. 1997, *ApJ*, 478, 527
- Kelly, B. C., Hughes, P. A., Aller, H. D., Aller, M. F. 2003, *ApJ*, 591, 695
- Kovalev, Y. Y., Lobanov, A. P., Pushkarev, A. B., Zensus, J. A. 2008, *A&A*, 483, 759
- Kroese, D. P., Porotsky, S., Rubinstein, R. Y. 2006, *Methodology and Computing in Applied Probability*, 8, 383
- Larwood, J. D. 1997, *MNRAS*, 290, 490
- Lind, K. R., Blandford, R. D. 1985, *ApJ*, 295, 358
- Lister, M. L., et al. 2009, *AJ*, 138, 1874
- Lobanov, A. P. 1998, *A&A*, 330, 79
- Marconi, A., Hunt, L. K. 2003, *ApJ*, 589, L21
- Margolin, L. 2004, *Annals of Operations Research*, 134, 201
- Monteiro, H., Dias, W. S., & Caetano, T. C. 2010, *A&A*, 516, 2
- Monteiro, H., Dias, W. S. 2011, *A&A*, 530, 91
- Mutel, R. L., Phillips, R. B., Su, B., Bucciferro, R. R. 1990, *ApJ*, 352, 81
- Mutel, R. L., & Denn, G. R. 2005, *ApJ*, 623, 79
- O’Sullivan, S. P., Gabuzda, D. C. 2009, *MNRAS*, 393, 429
- Papaloizou, J. C. B., Terquem, C. 1995, *MNRAS*, 274, 987
- Pauliny-Toth, I. I. K., Kellermann, K. I. 1966, *ApJ*, 146, 634
- Peacock, J. A., Readhead, A. C. S. 1988, *MNRAS*, 202, 615
- Pearson, T. J., Readhead, A. C. S. 1988, *ApJ*, 328, 114
- Polatidis, A. G., Wilkinson, P. N., Xu, W., Readhead, A. C. S., Pearson, T. J., Taylor, G. B., Vermeulen, R. C., 1995, *ApJS*, 98, 1
- Press, W., Teukolski, S., Vetterling, W., Flannery, B., 1997, *Numerical recipes in C: The Art of Scientific Computing*. Cambridge Univ. Press, Cambridge, 645
- Raiteri, C. M., et al. 2010, *A&A*, 524, 43
- Romero, G. E., Chajet, L., Abraham, Z., Fan, J. H. 2000, *A&A*, 360, 57
- Rubinstein, R. Y. 1997, *European Journal of Operational Research*, 99, 89
- Rubinstein, R. Y. 1999, *Methodology and Computing in Applied Probability*, 2, 127
- Savolainen, T., Homan, D. C., Hovatta, T., Kadler, M., Kovalev, Y. Y., Lister, M. L., Ros, E., Zensus, J. A. 2010, *A&A*, 512, 24
- Shapiro, S. L., Teukolsky, S. A. 1983, in *Black Holes, White Dwarfs and Neutron Stars*, John Wiley & Sons, New York, 476.
- Stirling, A. M., Cawthorne, T. V., Stevens, J. A., Jorstad, S. G., Marscher, A. P., Lister, M. L., Gómez, J. L., Smith, P. S., et al. 2003, *MNRAS*, 341, 405
- Tateyama, C. E., Kingham, K. A., Kaufmann, P., Piner, B. G., de Lucena, A. M. P., Botti, L. C. L., 1998, *ApJ*, 500, 810
- Tateyama, C. E., 2009, *ApJ*, 705, 877
- Vermeulen, R. C., Ogle, P. M., Tran, H. D., Browne, I. W. A., Cohen, M. H., Readhead, A. C. S., Taylor, G. B., Goodrich, R. W. 1995, *ApJ*, 452, L5
- Villata, M. et al. 2004, *A&A*, 424, 497
- Webb, J. R., Smith, A. G., Leacock, R. J., Fitzgibbons, G. L., Gombola, P. P., Sheppard, D. W. 1988, *AJ*, 95, 374
- Wild, V., Peacock, J. A., Lahav, O., Conway, E., Maddox, S., Baldry, I. K., Baugh, C. M., Bland-Hawthorn, J., Bridges, T., Cannon, R., et al. 2005, *MNRAS*, 356, 247
- Woo, J.-H., Urry, C. M. 2002, *ApJ*, 579, 530
- Wu, Q., Zou, Y., Cao, X., Wang, D.; Chen, L. 2011, *ApJ*, 740, L21

This paper has been typeset from a $\text{\TeX}/\text{\LaTeX}$ file prepared by the author.

8 SUPPORTING INFORMATION

Additional Supporting Information may be found in the online version of this article:

This additional material shows the projections on the plane of the sky of the precession helices generated from the model parameters listed in Table 1 over the entire observational period used in this work. We also display the 311 sky position of the jet knots of BL Lacertae that constrained our precession model. Note that precession helices describe the general trend of the observational data appropriately.

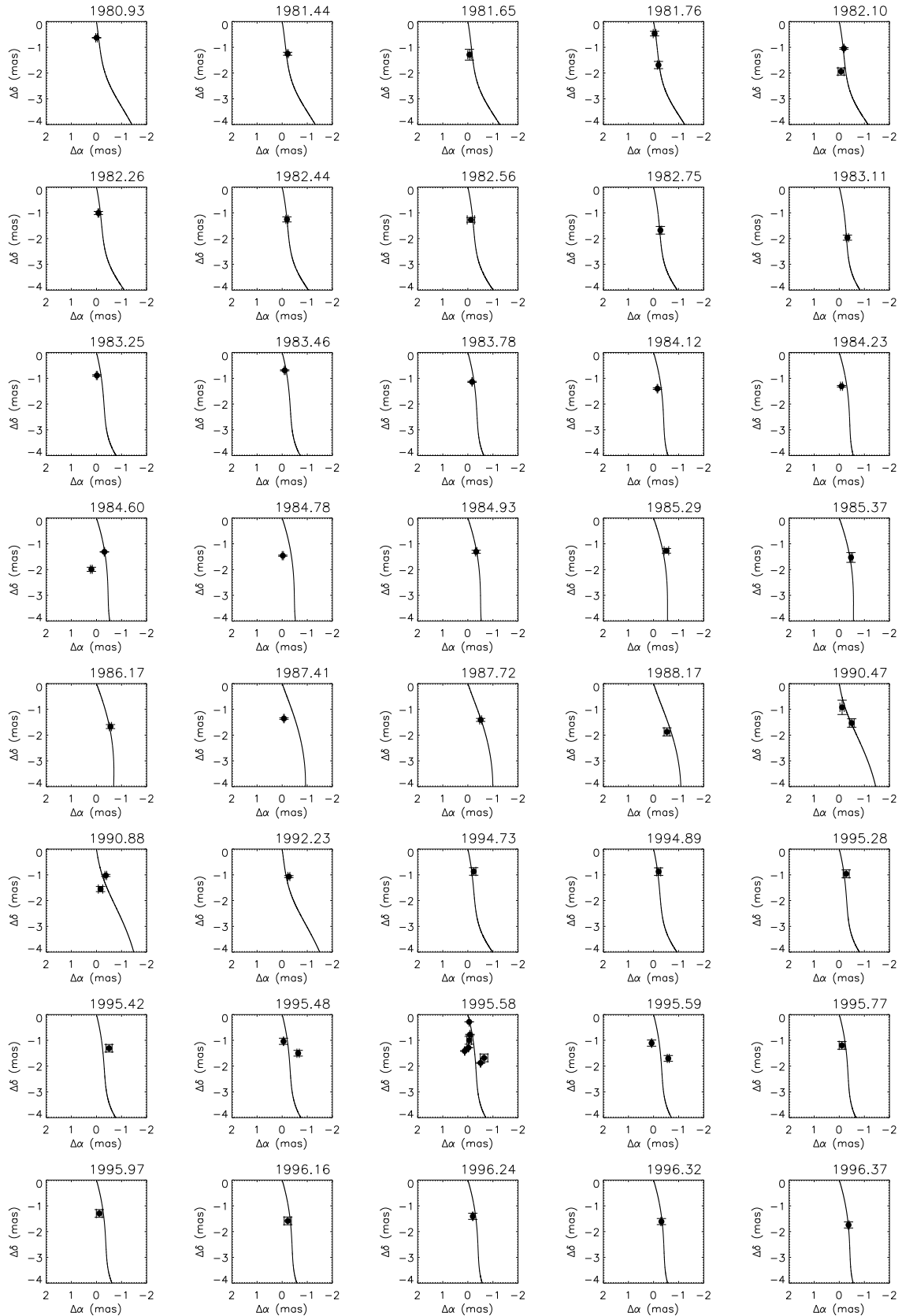


Figure 6. Changes in the jet orientation of BL Lacertae along the time due to the precession model parameters listed in Table 1. Solid lines represent snapshots of the precession helix, while the positions of the jet knots and their respective uncertainties are shown by black dots. Numbers at upper right corners of the panels are the corresponding observation epochs.

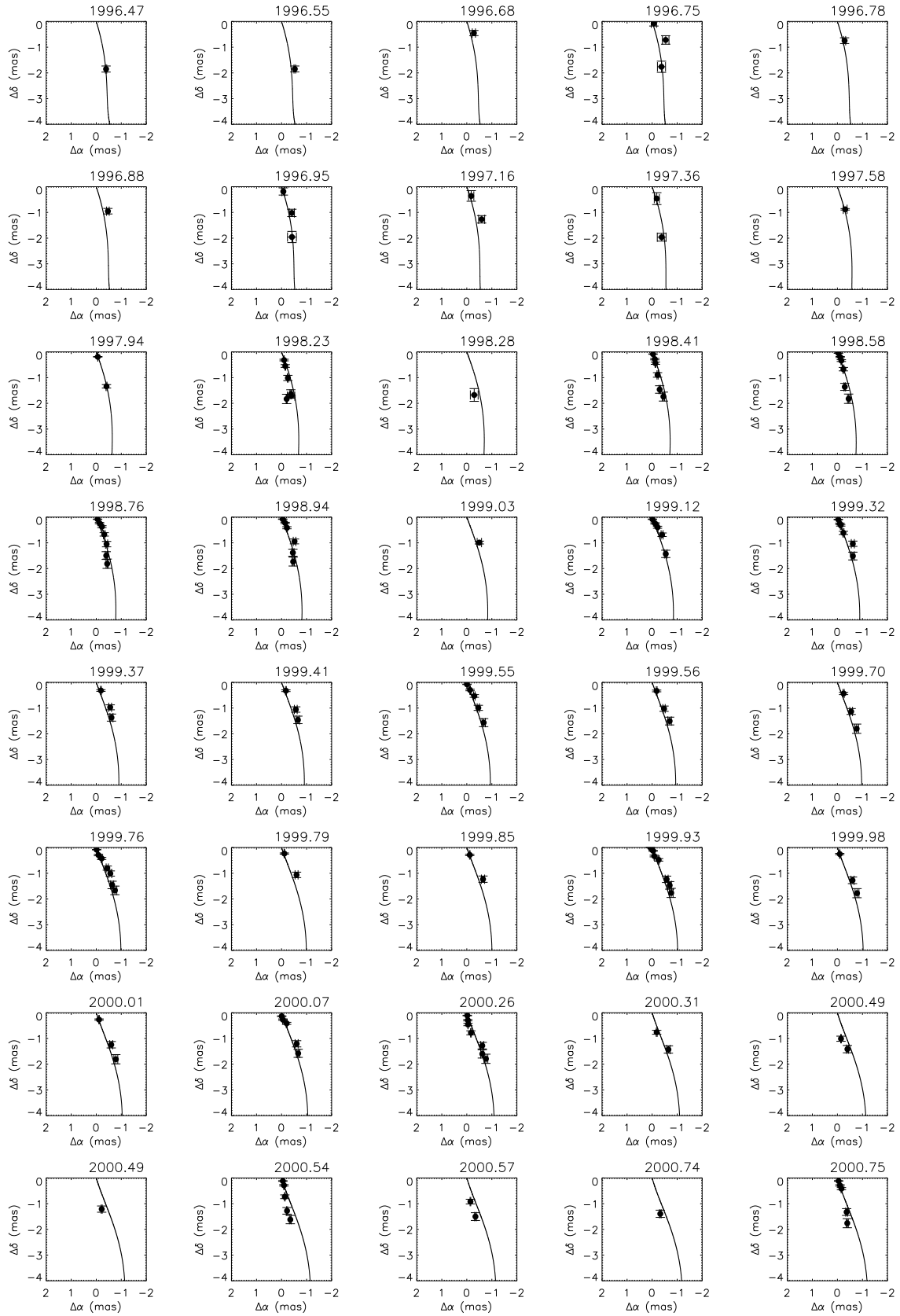


Figure 6. Continued.

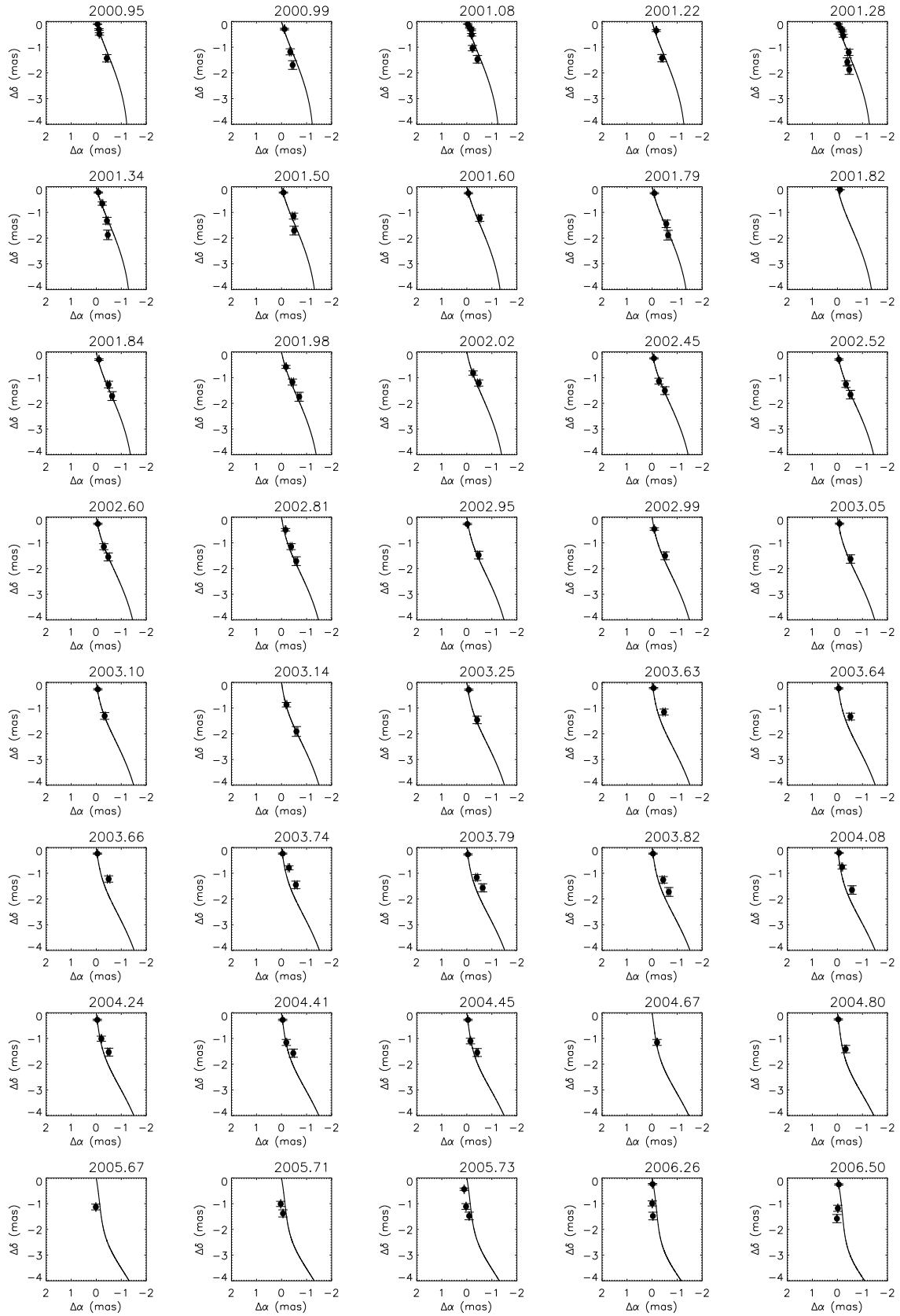


Figure 6. Continued.

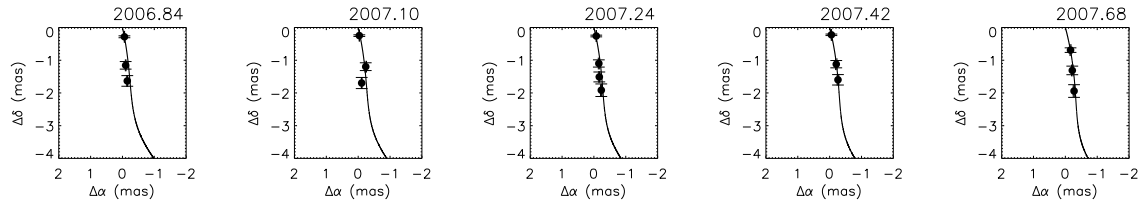


Figure 6. Continued.